

Effects of solvation and temperature on the energetics of BiVO₄ surfaces with varying composition for solar water splitting

Giacomo Melani^{1,*#}, Wennie Wang^{1,2},

Francois Gygi³, Kyoung-Shin Choi⁴, Giulia Galli^{1,5,6}

¹Pritzker School of Molecular Engineering, University of Chicago, IL, USA

gagalli@uchicago.edu

²McKetta Department of Chemical Engineering, University of Texas at Austin, TX, USA

³Department of Computer Science, University of California Davis, CA, USA

⁴Department of Chemistry, University of Wisconsin-Madison, WI, USA

⁵Materials Science Division, Argonne National Laboratory, IL, USA

⁶Department of Chemistry, University of Chicago, IL, USA

#present address: Istituto di Chimica dei Composti Organometallici, Consiglio Nazionale delle Ricerche, Pisa, Italy

ABSTRACT

Photoelectrodes used in solar water splitting must operate in aqueous media. However, computational studies that explicitly compare the dry and solvated photoelectrode energetics at finite temperature and the impact of photoelectrode surface composition and surface defects are lacking. Here, we used first-principles molecular dynamics simulations to investigate the solvation and thermal effects on the energetics of the BiVO₄(010) surface with different surface compositions and oxygen vacancies, a common defect responsible for the intrinsic n-type behavior of BiVO₄. We find that the alignment of the photoelectrode electronic bands with the water redox potentials is modified in the presence of water, and that solvation effects and thermal fluctuations are more prominent for Bi-rich surfaces, especially so in the presence of oxygen vacancies. Our results provide a detailed understanding of the behavior of BiVO₄ photoanodes operating in aqueous media, as a function of surface composition, and are directly comparable with experiments.

Oxide semiconductors are interesting materials for use as photoelectrodes in solar water splitting, as they exhibit compositional flexibility and relatively good stability in aqueous environments¹. Recently, the importance of understanding and optimizing surface structure and composition, in addition to the bulk properties of the oxide photoelectrode, has been demonstrated by various studies²⁻⁹. For example, we showed that epitaxially-grown BiVO₄ (010) photoelectrodes with the stoichiometric (Bi:V ratio of 1:~1) and Bi-rich outermost layer have considerably different surface energetics that directly impact their photoelectrochemical properties; the band edges and work function of the Bi-rich BiVO₄ (010) photoelectrode are closer to the vacuum level than those of the stoichiometric surface, resulting in a more pronounced band bending under any applied potential, which in turn leads to a better electron-hole separation and hence to enhanced photocurrent generation¹⁰.

Unlike photoelectrodes used in solid-state solar cells, photoelectrodes used in water-splitting photoelectrochemical cells must operate in aqueous solutions. Thus, an accurate understanding of the impact of the aqueous environment on photoelectrode surfaces requires an understanding of how solvation affects the photoelectrode energetics and electronic properties. However, many computational studies assume vacuum conditions when investigating photoelectrodes. For example, the properties of epitaxially grown BiVO₄ (010) photoelectrodes with Bi-rich surfaces were computationally investigated using only dry surfaces¹⁰ while several studies of the solvated stoichiometric ones have appeared in the literature¹¹⁻¹⁵. When a ternary oxide with the formula A_xB_yO_z is prepared, the surface A:B ratio can often be different from the bulk A:B ratio and varies by the synthesis method. Thus, understanding how surfaces with different composition are affected by solvation is of great interest and importance. Another important factor when considering solvation effects is the presence of defects on the photoelectrode surfaces. For example, oxygen vacancies are common defects in n-type oxides such as BiVO₄ and their presence on the surface may alter the way the surface and water molecules interact, thereby changing the surface energetics.

In order to address our lack of understanding of solvation and finite temperature effects as a function of surface composition, we investigate the electronic, structural, and vibrational properties of dry and solvated BiVO₄ (010) surfaces and we compare results for the stoichiometric and Bi-rich surfaces, with and without oxygen vacancies. The experimentally observed photoelectrochemical properties of BiVO₄ (010) with different surface compositions (stoichiometric surface where Bi:V is 1:~1 vs Bi-rich surface) have been well documented¹⁰. Hence, the computational results reported in this study can be validated by our previous experimental studies, while providing a detailed understanding of the fundamental properties of BiVO₄ photoanodes operating in aqueous media. Our results show that the impact of solvation and temperature is different for the stoichiometric and Bi-rich facets, and that the finite temperature fluctuations of the electronic defect levels associated to oxygen vacancies are enhanced in the Bi-rich surface, compared to the stoichiometric one. Hence explicit studies of solvation as a function of surface morphology are necessary to gather a full understanding of the properties of bismuth vanadate photoelectrodes.

We carried out first-principles molecular dynamics simulations (FPMD) at the meta-GGA level¹⁶ of theory and investigated the electronic properties of selected snapshots, using dielectric-dependend hybrid (DDH) functionals¹⁷. Specifically, we used the (SCAN) functional and the Qbox code (versions 1.74.2 and 1.75.0)¹⁸ (see SI for details). A total of twelve trajectories of ~ 8 ps each were obtained (six for the pristine stoichiometric and six for the Bi-rich BiVO_4 /water interfaces, respectively), starting from different initial configurations. The total simulations time is consistent with that considered in previous works¹¹. The initial configurations from which multiple trajectories were started, were chosen after running NPT (constant pressure, P and temperature T) simulations (average length, 6 ps) to optimize the average distance between the liquid and the solid surface (see Fig. S2). Two additional trajectories of 6 ps each were generated for each of the BiVO_4 interfaces (stoichiometric and Bi-rich) with oxygen vacancies, starting from pre-equilibrated trajectories of the corresponding pristine systems. For each of the trajectories we verified that the total energy and temperature were properly equilibrated. In order to study the electronic structure of the BiVO_4 substrate, we performed calculations with the DDH functional on SCAN trajectories. The fraction of mixing of exact and local exchange was set to $\alpha = 1/\varepsilon_\infty = 1/6.9$, where ε_∞ is the long-wavelength dielectric constant of BiVO_4 . In our prior work, we verified the accuracy of the DDH functional for characterizing the electronic structure of BiVO_4 through a study of oxygen vacancies in the bulk²⁰ and at the surface²¹, including a comparison of computed values to experiments conducted on epitaxially-grown and single-crystalline thin film samples^{14,21}.

We modeled bismuth vanadate in contact with heavy water (64 D_2O molecules) instead of light water for computational convenience (use of a larger time step than in the case of light water) and we used $(2 \times 2 \times 2)$ symmetric slab models of composition $\text{Bi}_{16}\text{V}_{16}\text{O}_{64}$ and $\text{Bi}_{16}\text{V}_{8}\text{O}_{56}\text{D}_{24}$ (4 BVO layers) and $\text{Bi}_{32}\text{V}_{32}\text{O}_{128}$ and $\text{Bi}_{32}\text{V}_{24}\text{O}_{120}\text{D}_{24}$ (8 BVO layers) to represent the stoichiometric and the bismuth-rich surfaces, respectively (see SI for a study of finite size effects). The Bi-rich model used in our previous study¹⁰ was constructed by removing all V atoms from the top-most layer of the stoichiometric surface and terminating the topmost layer with Bi atoms. Experimentally, in order to obtain a Bi-rich sample, the stoichiometric sample is treated in a strongly basic solution for an appropriate duration to remove the top-most vanadium atoms¹⁰. In such a OH-rich basic aqueous solution, the remaining surface Bi atoms are expected to be hydroxylated. We optimized the geometry of the Bi-rich surface where Bi is terminated with one, two and three OD groups and found that the one with three groups was the most stable. Hence, to closely mimic the experimental Bi-rich sample, the Bi-rich surface model used here consists of stoichiometric BiVO_4 layers, covered by four Bi $(\text{OD})_3$ groups on each surface of the slab. A ball and stick representation of the pristine models used here is shown in Figure 1.

To study the effect of defects on the properties of the BiVO_4 /water interfaces, we considered the presence of surface oxygen vacancies, building on our previous work where we

investigated vacancies in the absence of water^{20,21}. We considered the same symmetric slabs described above and removed an oxygen atom from each of the outermost layers, formally removing two oxygen atoms from the slab.

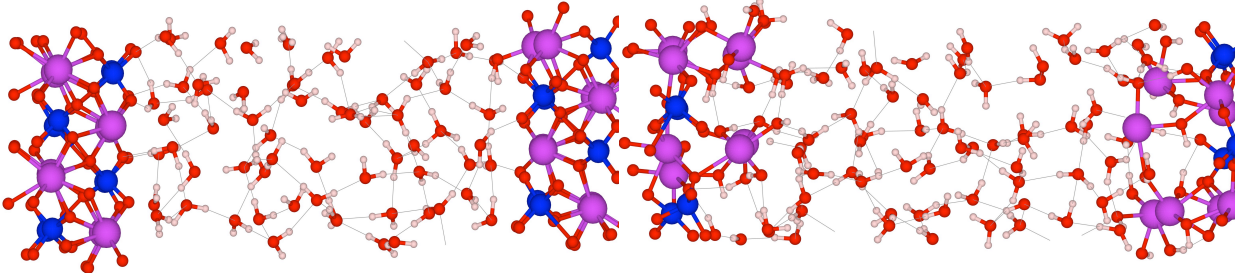


Figure 1 Structural models (balls and stick representation) of the stoichiometric (left) and bismuth-rich BiVO₄ (010) surfaces in contact with deuterated water (64 D₂O molecules). We used periodic boundary conditions with a symmetric slab and hence in our supercell two surfaces exposed to water are present. For ease of visualization we show the 64 water molecules at the center of the slab. Color coding: oxygen atoms (red), vanadium (blue), bismuth (purple) and hydrogen (grey).

We discuss the results of our simulations starting from the structural and vibrational properties of water in contact with BiVO₄, beginning with the stoichiometric surface.

In agreement with our previous results obtained at the PBE+U¹⁴ level of theory, we found that molecular adsorption of water is energetically preferred with respect to dissociative adsorption on the stoichiometric surface when using the SCAN functional (We considered the same molecular and dissociative configurations discussed in Ref. 14, Table 1). The SCAN functional yields slightly larger adsorption energies than PBE+U, possibly due to the partial inclusion of short-range van der Waals interactions. We then investigated whether dissociative adsorption is also thermodynamically unfavorable for the fully solvated surface, i.e. when the surface is entirely covered by water molecules. To this end, we started some of our FPMD simulations from configurations of pre-dissociated D₂O molecules on the surface. We observed that most dissociated fragments present at the interface did recombine to form water molecules, which were then molecularly adsorbed on the surface, in agreement with previous ab-initio simulations²² and with our own results for one water monolayer¹⁴.

Specifically, on the stoichiometric surface we find that oxygen atoms from water molecules adsorb on the topmost bismuth atoms, interacting with Bi through their lone electronic pairs. Water molecules also adsorb by donating hydrogen bonds to surface oxygen atoms.

In the case of the bismuth-rich (010) surface, where the topmost Bi-(OD)₃ groups can receive and donate hydrogen bonds to water, the surface-liquid interactions are different from those on the stoichiometric surface. The Bi-rich surface forms temporary hydrogen bonds with water molecules using its terminal deuterated hydroxyl groups which sterically hinder the adsorption of molecular water. While the stoichiometric surface exhibits direct molecular

adsorption, the Bi-rich surface features fluctuating hydrogen bonds, which might lead to faster diffusion of molecules in the second water layer.

We also computed the vibrational density of states (VDOS) from the velocity-velocity autocorrelation function, which can be easily decomposed into atomic contributions from different species. Although the spectra of the stoichiometric and Bi-rich surface are similar within our statistical resolution (see Fig. S4), it is interesting to note that the frequency of the O-D stretching modes of the Bi-OD groups fall approximately in the same range as those of the asymmetric stretching modes of D₂O. Hence, we expect a slight enhancement of the asymmetric peak for the Bi-rich surface that could be detected by surface-sensitive vibrational measurements, such as sum frequency generation (SFG) measurements²⁴. If these experiments are feasible, they would be a useful tool to assess the type of aqueous interfaces formed under different experimental conditions.

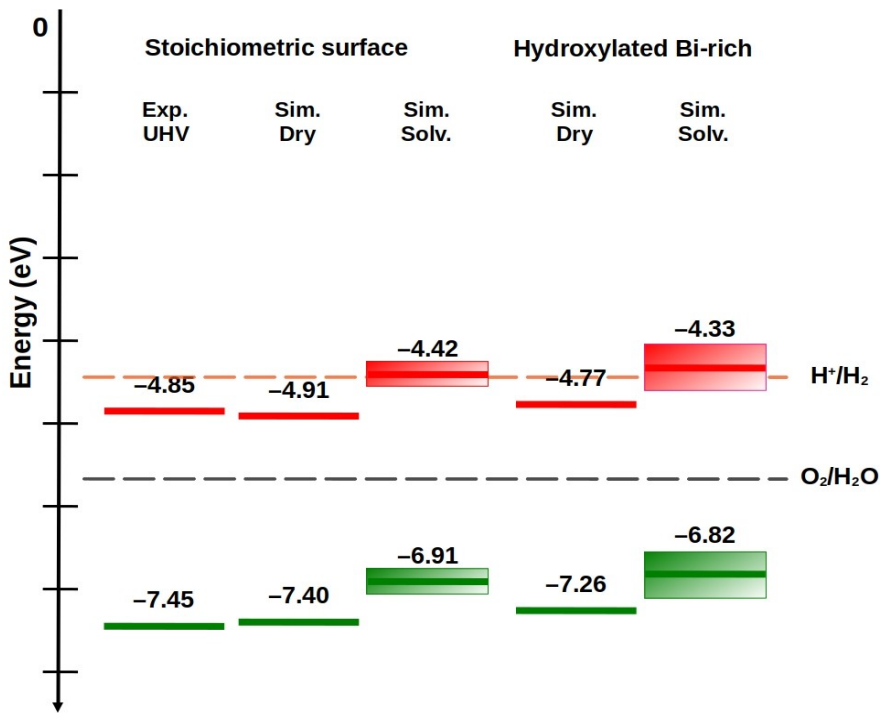


Figure 2 Band alignment of the valence band maxima (VBM, in green) and conduction band minima (CBM, in red) with respect to vacuum level for stoichiometric and hydroxylated- Bi-rich BiVO₄(010). We report experimental values of single-crystalline BiVO₄ obtained in ultra-high-vacuum conditions (Exp. UHV) from Refs.[10,32]. and results obtained from first-principles simulations (Sim.) for the dry and solvated (Solv.) stoichiometric and Bi-rich surfaces. Electronic energy levels are computed at the DDH level of theory on 20 snapshots obtained from SCAN/FPMD trajectories at 330 K for both systems. Thermal fluctuations of V(C)BM values are indicated with green and red rectangles, yielding a 150 and 280 meV spread for the stoichiometric and bismuth-rich interfaces, respectively.

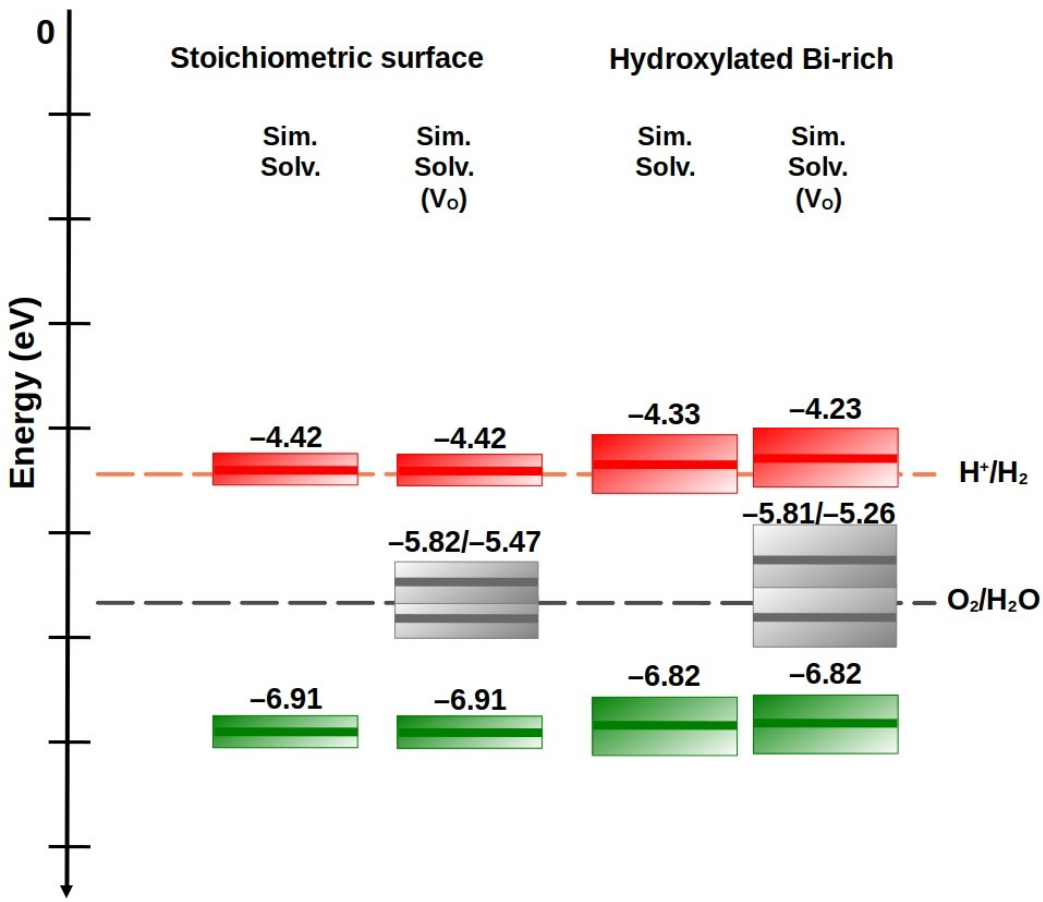


Figure 3

Band alignment of the valence band maxima (VBM, in green) and conduction band minima (CBM, in red) relative to the vacuum level for solvated (Solv.) stoichiometric and hydroxylated- Bi-rich BiVO₄(010), in the presence of oxygen vacancies (V₀), as obtained from first-principles simulations (Sim.). Electronic energy levels are computed at the DDH level of theory from 20 snapshots obtained from SCAN/FPMD trajectories at 330 K for both systems. Thermal fluctuations of V(C)BM values and defect levels are indicated with green, red and gray rectangles, respectively. The defect levels were computed at the SCAN level of theory, and they were positioned relative to the top of the vacuum-referenced valence band obtained in Fig.2.

We now turn to the discussion of the electronic properties of solvated stoichiometric and Bi-rich surfaces, in particular the effect played by solvation and surface composition on the band edge positions of the photoelectrode.

Following previous work^{10,12,14,21,25-30}, we determined the absolute valence band maximum (VBM) and conduction band minimum (CBM) positions with respect to the vacuum level, and we then aligned them to the water electrochemical potentials (see SI for details).

Figures 2 and 3 summarize our results for pristine and defective BiVO₄, respectively; the electronic structure was obtained using the DDH hybrid functional on SCAN trajectories and using 8 layer slabs to represent the surface (see SI). Note that we adopted corrections due to spin-orbit coupling, excitonic effects, and nuclear quantum effects, which are taken from path-integral ab initio molecular dynamics simulations and computed optical spectra based

on GW/BSE for BiVO_4 in Ref. 21. For BiVO_4 , these corrections lead to a shift in the band edge positions ($\Delta\text{VBM} = +0.50$ eV, $\Delta\text{CBM} = -0.43$ eV). Such corrections are numerically different from those that we previously used to study the dry (010) BiVO_4 surface^{21,31} as thermal fluctuations are already included in our finite-temperature FPMD simulations and were thus omitted from the corrections proposed in Ref. 21.

We start by describing the surfaces in the absence of defects. Figure 2 compares the band alignments of stoichiometric and hydroxylated Bi-rich BiVO_4 (010) with dry and solvated surfaces (see SI) so that the effects of solvation on the band edge positions are explicitly shown.

For dry, UHV-like conditions, we find that the VBM of the stoichiometric surface is located at 7.40 eV from vacuum, in agreement with previously reported values²¹ computed at the PBE+U (2.7 eV) level and with photo-emission experiments (7.45 eV)³². When considering a solvated stoichiometric surface, we find that the VBM moves up to 6.91 eV and the CBM moves up to 4.42 eV. Such a shift in the electronic band edges due to solvation is consistent with what has been reported for other oxides³³.

We note that in our previous study¹⁰, the positions of the VBM and CBM levels of the dry bismuth-rich surface were calculated without hydroxylation or solvation, and hence their positions were unrealistically close to the vacuum level (at 4.63 eV and 2.49 eV from vacuum, respectively); in particular, the VBM position was even higher (less positive in the reversible hydrogen electrode scale) than that of the water oxidation potential, which is unrealistic. However, when the surface is hydroxylated, namely terminated by Bi-(OD)_3 , we find that the VBM and CBM levels are lowered and are positioned closer to but not above the oxygen evolution reaction (OER) potential. At the same time, the CBM and VBM of the dry, hydroxylated Bi-rich surface are still slightly higher than those of the dry stoichiometric surface (Figure 3). For example, the VBM of the dry, hydroxylated Bi-rich surface is higher by 0.14 eV: this value is comparable to the experimentally observed difference (0.15 eV) between the VBM levels of these two samples, which was determined by XPS under vacuum conditions¹⁰.

When the surface is fully solvated, the VBM and CBM levels of the hydroxylated Bi-rich surface moves up slightly closer to the vacuum level as in the case of the stoichiometric sample, and hence they remain higher than those of the solvated stoichiometric surface, consistent with the experimental results discussed in detail below.

The CBM of the solvated, hydroxylated Bi-rich surface shown in Figure 2 is slightly above the HER potential (-4.44 eV)³⁴. We note that this result was obtained by carrying out MD simulations of a Bi-rich surface with the top-most layer having only Bi and no V (i.e., equivalent to having 4 Bi atoms at the top-most layer). However, in experiments, Bi-rich samples may still contain some V atoms on the surface and the coordination of Bi may be different from that used in our calculations. We expect that both the surface Bi:V ratio and their detailed coordination environments can impact the exact CBM position of experimental samples. For example, the experimental Bi-rich sample prepared in our previous study¹⁰ had

the Bi:V ratio of 79:21, and our previous calculations showed that the band edge positions shift closer to the vacuum and vary linearly with increasing Bi:V ratio¹⁰. Therefore, we repeated some of our calculations using 75% Bi-rich substrates and we observed a slight lowering of the CBM below the hydrogen evolution potential, consistent with the expectations that Bi-rich surfaces may indeed contain some V atoms at the surface and that the BiVO₄ surface is not HER active. We also observed a modest lowering of the VBM when decreasing the Bi-concentration at the surface.

It is important to note that thermal fluctuations have a larger influence on the electronic structure of the Bi-rich surface relative to the stoichiometric one, as shown in Figure 3. This difference is shown by the width of the colored rectangles, whose edges show the energetic range of the fluctuations. The increased amplitude in the Bi-rich surface is due to the presence of Bi-OD groups and dynamically gives rise to a more favorable positions of the CBM and VBM for water splitting.

Next, we consider the effect of the surface O vacancy (V₀) on the solvation effects. In BiVO₄, oxygen vacancies are a common source of n-type dopants, as in many semiconducting oxides. In a previous work by our group²¹, an extensive analysis of oxygen vacancies in bulk and surface bismuth vanadate was reported, shedding light on the role of this type of defect on the electronic structure of BiVO₄.

Here, we considered a neutral V₀ where an oxygen atom is removed from a VO₄³⁻ anion and the remaining VO₃³⁻ species has two unpaired electrons in the vanadium 3d-orbitals (V³⁺ with a d² electronic configuration), making the oxygen vacancy an n-type dopant. Due to this change in composition and electronic structure, the atoms surrounding the anion vacancy undergo a structural deformation at finite temperature, and the geometry is stabilized by hydrogen bonding with D₂O molecules.

Figure 2 compares the band alignments of the solvated surfaces of stoichiometric and hydroxylated Bi-rich BiVO₄ (010) without and with V₀ so that the effects of V₀ on the band edge positions are explicitly shown. First, the presence of V₀ does not shift the VBM and CBM of the stoichiometric surface. However, the presence of V₀ on the Bi-rich surface further shifts the CBM toward the vacuum level by 0.1 eV while the VBM remains the same. This shows that the effect of V₀ on the solvation effects vary with the surface composition. This also means that in order to accurately elucidate the effect of V₀ on the solvation effects for any given oxide photoelectrode³⁵, knowing the surface composition and using a surface model mimicking the experimental surface is critical to obtain the most meaningful results.

The band diagrams of the solvated models with V₀ (Figure 3) are those most relevant to use to interpret the experimentally observed photoelectrochemical behavior of the two samples under illumination. In our previous study, we compared BiVO₄ (010) photoelectrodes with stoichiometric and Bi-rich surfaces for photoelectrochemical sulfite oxidation¹⁰. Sulfite is a hole scavenger with fast interfacial oxidation kinetics unlike water whose oxidation kinetics on the BiVO₄ surface are much slower^{32,36}. Therefore, during photoelectrochemical sulfite oxidation the surface recombination of holes can be assumed to be negligible. As a result, the

photocurrent onset potential for sulfite oxidation can be considered as the apparent flat band potential of the photoanode³⁶. Furthermore, the difference in photocurrent between the two samples can be directly related to the difference in the number of surface-reaching holes, which results from the effect of surface composition on interfacial energetics and band bending. Our previous experimental results showed that the sample with the Bi-rich surface has a more negative photocurrent onset potential and significantly enhances photocurrent for sulfite oxidation¹⁰. Previously, these differences were interpreted with the band diagrams obtained without including the effect of hydroxylation of the Bi-rich surface, the presence of V_0 , or solvation effects. Qualitatively, our previous and current results both show that the Bi-rich surface has band edge positions and work function closer to the vacuum level than those of the stoichiometric surface. This qualitatively explains the fact that the sample with the Bi-rich surface is expected to have a greater degree of band bending under any given potential, thereby leading to a greater degree of electron-hole pair separation, compared to the stoichiometric surface, and thus generating an enhanced photocurrent for sulfite oxidation. However, previous calculations were not quantitatively accurate and neglected solvation and defect effects. The current results reported in Figure 3 show more accurate band positions for the two samples with a difference that explains the experimentally observed behaviors.

As seen in Figure 2, two in-gap states corresponding to the two oxygen vacancies introduced in the sample appear for both systems, with the spacing between these defect levels depending on the surface composition. For the stoichiometric interface, the defect levels are separated by about 350 meV, while in the Bi-rich case they are separated by 800 meV and are subject to larger thermal fluctuations. Both defect levels are occupied in the case of neutral vacancies, formally shifting the Fermi level upward.

We note that when BiVO_4 is used as a photoanode for water oxidation in an aqueous solution under illumination, some of the defect levels will be emptied, due to the recombination of the electrons in these levels with the photogenerated holes in the VBM. If the resulting empty defect levels are located below the OER potential, they may mediate the electron transfer from water to the VB of BiVO_4 (equivalent to hole transfer from the VB of BiVO_4 to water) during photooxidation of water, affecting the rate of OER. Physically, the V_0 may also offer a site where water adsorbs differently than on the non-defective surface (i.e., by dissociative adsorption), affecting the OER mechanism and potentially allowing for a more facile water oxidation¹²⁻¹⁴.

However, the BiVO_4 surface is poorly catalytic for OER and is always paired with an oxygen evolution catalyst when used for solar water oxidation³⁷. Then, the position of the defect levels relative to the redox level of the catalytic center in the OER catalyst will be important as the position of the defect levels can impact how well the holes can be transferred from BiVO_4 to the OER catalyst, and what fraction of the holes will be lost at the interface due to interfacial electron-hole recombination. The impact of the defect levels studied here (Figure 2) and their interaction with OER catalysts merits further investigation, and it is expected to

vary depending on the choice of the OER catalyst. Nevertheless, our study clearly demonstrates that even with the same type of defect (in this case, V_0), the solvation effects on the positions and fluctuations of the defect levels and band edges vary depending on the surface composition of BiVO_4 , all of which will influence differently the OER performance and the way BiVO_4 photoanodes interact with an OER catalyst.

In summary, we have investigated how solvation, finite temperature, and the presence of defects influence the structural, vibrational, and electronic structure of the BiVO_4 (010) surface as a function of the surface composition. Most computational studies of BiVO_4 surfaces have been limited to static calculations at 0 K and focus almost exclusively on the stoichiometric surface. Similarly, solvation properties have been studied in only a few papers, and limited to stoichiometric surfaces. Here we investigated both the stoichiometric surface, which is a commonly assumed surface composition, and Bi-rich surfaces, which are known experimentally to yield photoelectrodes of superior performance. Uniquely, our study explicitly reveals the separate and combined distinct effects of solvation, finite temperature, and the presence of surface oxygen vacancies on the surface electronic structure and their important dependence on surface composition. Notably, the electronic surface of the Bi-rich surface demonstrates a greater sensitivity to solvation, thermal fluctuations, and the presence of surface defects. Indeed, our results, obtained with first-principles MD simulations, reveal the beneficial effect of solvation in leading to an energetic shift of the electronic bands and consequently more favorable position of the VBM and CBM with respect to the OER potential in comparison to those of the dry surfaces. The presence of V_0 in combination with thermal fluctuations also contribute to a more favorable electronic structure of Bi-rich BiVO_4 (010) for solar water splitting. Our results also provide accurate band positions that can explain the previously observed experimental result where BiVO_4 (010) with the Bi-rich surface exhibited a pronounced band bending and enhanced electron-hole separation, resulting in higher photocurrent generation compared to BiVO_4 (010) with the stoichiometric surface.

Supporting information

Details on calculation of structural properties of water, vibrational spectra and band alignments.

Acknowledgements

We thank Chenyu Zhou and Mingzhao Liu for many useful discussions and Jorge Sofo and Alessandro Fortunelli for discussions and continuous support. This work was funded by the National Science Foundation (NSF) under grant no. CHE-2054986.

References

- (1) Lee, D. K.; Lee, D.; Lumley, M. A.; Choi, K.-S. Progress on Ternary Oxide-Based Photoanodes for Use in Photoelectrochemical Cells for Solar Water Splitting. *Chem. Soc. Rev.* **2019**, *48* (7), 2126–2157. <https://doi.org/10.1039/C8CS00761F>.
- (2) Sharp, I. D.; Cooper, J. K.; Toma, F. M.; Buonsanti, R. Bismuth Vanadate as a Platform for Accelerating Discovery and Development of Complex Transition-Metal Oxide Photoanodes. *ACS Energy Lett.* **2017**, *2* (1), 139–150. <https://doi.org/10.1021/acsenergylett.6b00586>.
- (3) Zachäus, C.; Abdi, F. F.; Peter, L. M.; Van De Krol, R. Photocurrent of BiVO₄ Is Limited by Surface Recombination, Not Surface Catalysis. *Chem. Sci.* **2017**, *8* (5), 3712–3719. <https://doi.org/10.1039/C7SC00363C>.
- (4) Nguyen, T. D.; Nguyen, V.-H.; Nanda, S.; Vo, D.-V. N.; Nguyen, V. H.; Van Tran, T.; Nong, L. X.; Nguyen, T. T.; Bach, L.-G.; Abdullah, B.; Hong, S.-S.; Van Nguyen, T. BiVO₄ Photocatalysis Design and Applications to Oxygen Production and Degradation of Organic Compounds: A Review. *Environ. Chem. Lett.* **2020**, *18* (6), 1779–1801. <https://doi.org/10.1007/s10311-020-01039-0>.
- (5) Zhou, L.; Shinde, A.; Guevarra, D.; Haber, J. A.; Persson, K. A.; Neaton, J. B.; Gregoire, J. M. Successes and Opportunities for Discovery of Metal Oxide Photoanodes for Solar Fuels Generators. *ACS Energy Lett.* **2020**, *5* (5), 1413–1421. <https://doi.org/10.1021/acsenergylett.0c00067>.
- (6) Kim, T. W.; Ping, Y.; Galli, G. A.; Choi, K. S. Simultaneous Enhancements in Photon Absorption and Charge Transport of Bismuth Vanadate Photoanodes for Solar Water Splitting. *Nat. Commun.* **2015**, *6*, 8769. <https://doi.org/10.1038/ncomms9769>.
- (7) Ding, K.; Chen, B.; Fang, Z.; Zhang, Y.; Chen, Z. Why the Photocatalytic Activity of Mo-Doped BiVO₄ Is Enhanced: A Comprehensive Density Functional Study. *Phys. Chem. Chem. Phys.* **2014**, *16* (26), 13465. <https://doi.org/10.1039/c4cp01350f>.
- (8) Tachikawa, T.; Ochi, T.; Kobori, Y. Crystal-Face-Dependent Charge Dynamics on a BiVO₄ Photocatalyst Revealed by Single-Particle Spectroelectrochemistry. *ACS Catal.* **2016**, *6* (4), 2250–2256. <https://doi.org/10.1021/acscatal.6b00234>.
- (9) Zhu, J.; Fan, F.; Chen, R.; An, H.; Feng, Z.; Li, C. Direct Imaging of Highly Anisotropic Photogenerated Charge Separations on Different Facets of a Single BiVO₄ Photocatalyst. *Angew. Chem. Int. Ed.* **2015**, *54* (31), 9111–9114. <https://doi.org/10.1002/anie.201504135>.
- (10) Lee, D.; Wang, W.; Zhou, C.; Tong, X.; Liu, M.; Galli, G.; Choi, K. S. The Impact of Surface Composition on the Interfacial Energetics and Photoelectrochemical Properties of BiVO₄. *Nat. Energy* **2021**, *6* (3), 287–294. <https://doi.org/10.1038/s41560-021-00777-x>.
- (11) Ambrosio, F.; Wiktor, J.; Pasquarello, A. PH-Dependent Surface Chemistry from First Principles: Application to the BiVO₄(010)-Water Interface. *ACS Appl. Mater. Interfaces* **2018**, *10* (12), 10011–10021. <https://doi.org/10.1021/acsami.7b16545>.
- (12) Wiktor, J.; Pasquarello, A. Electron and Hole Polarons at the BiVO₄-Water Interface. *ACS Appl. Mater. Interfaces* **2019**, *11* (20), 18423–18426. <https://doi.org/10.1021/acsami.9b03566>.
- (13) Hermans, Y.; Murcia-López, S.; Klein, A.; Jaegermann, W. BiVO₄ Surface Reduction upon Water Exposure. *ACS Energy Lett.* **2019**, *4* (10), 2522–2528. <https://doi.org/10.1021/acsenergylett.9b01667>.
- (14) Wang, W.; Favaro, M.; Chen, E.; Trotochaud, L.; Bluhm, H.; Choi, K. S.; Van De Krol, R.; Starr, D. E.; Galli, G. Influence of Excess Charge on Water Adsorption on the BiVO₄(010) Surface. *J. Am. Chem. Soc.* **2022**, *144* (37), 17173–17185. <https://doi.org/10.1021/jacs.2c07501>.
- (15) Tao, J.; Liu, G.; Liu, T. Ab Initio Molecular Dynamics Simulation the Electron and Hole Polarons at the Interface between Water and the Surfaces of BiVO₄. *J. Phys. Chem. C* **2024**, *128* (13), 5680–5685. <https://doi.org/10.1021/acs.jpcc.3c06847>.
- (16) Sun, J.; Ruzsinszky, A.; Perdew, J. P. Strongly Constrained and Appropriately Normed Semilocal Density Functional. *Phys. Rev. Lett.* **2015**, *115* (3), 036402. <https://doi.org/10.1103/PhysRevLett.115.036402>.

(17) Skone, J. H.; Govoni, M.; Galli, G. Self-Consistent Hybrid Functional for Condensed Systems. *Phys. Rev. B* **2014**, *89* (19), 195112. <https://doi.org/10.1103/PhysRevB.89.195112>.

(18) Gygi, F. Architecture of Qbox: A Scalable First-Principles Molecular Dynamics Code. *IBM J. Res. Dev.* **2008**, *52* (1.2), 137–144. <https://doi.org/10.1147/rd.521.0137>.

(19) Lacout, M. D.; Gygi, F. Ensemble First-Principles Molecular Dynamics Simulations of Water Using the SCAN Meta-GGA Density Functional. *J. Chem. Phys.* **2019**, *151* (16), 164101. <https://doi.org/10.1063/1.5124957>.

(20) Seo, H.; Ping, Y.; Galli, G. Role of Point Defects in Enhancing the Conductivity of BiVO₄. *Chem. Mater.* **2018**, *30* (21), 7793–7802. <https://doi.org/10.1021/acs.chemmater.8b03201>.

(21) Wang, W.; Strohbeen, P. J.; Lee, D.; Zhou, C.; Kawasaki, J. K.; Choi, K. S.; Liu, M.; Galli, G. The Role of Surface Oxygen Vacancies in BiVO₄. *Chem. Mater.* **2020**, *32* (7), 2899–2909. <https://doi.org/10.1021/acs.chemmater.9b05047>.

(22) Oshikiri, M.; Boero, M. Water Molecule Adsorption Properties on the BiVO₄ (100) Surface. *J. Phys. Chem. B* **2006**, *110* (18), 9188–9194. <https://doi.org/10.1021/jp0555100>.

(23) Huang, P.; Pham, T. A.; Galli, G.; Schwegler, E. Alumina(0001)/Water Interface: Structural Properties and Infrared Spectra from First-Principles Molecular Dynamics Simulations. *J. Phys. Chem. C* **2014**, *118* (17), 8944–8951. <https://doi.org/10.1021/jp4123002>.

(24) Calegari Andrade, M. F.; Ko, H.-Y.; Car, R.; Selloni, A. Structure, Polarization, and Sum Frequency Generation Spectrum of Interfacial Water on Anatase TiO₂. *J. Phys. Chem. Lett.* **2018**, *9* (23), 6716–6721. <https://doi.org/10.1021/acs.jpclett.8b03103>.

(25) Ambrosio, F.; Miceli, G.; Pasquarello, A. Redox Levels in Aqueous Solution: Effect of van Der Waals Interactions and Hybrid Functionals. *J. Chem. Phys.* **2015**, *143* (24), 244508. <https://doi.org/10.1063/1.4938189>.

(26) Guo, Z.; Ambrosio, F.; Chen, W.; Gono, P.; Pasquarello, A. Alignment of Redox Levels at Semiconductor-Water Interfaces. *Chem. Mater.* **2018**, *30* (1), 94–111. <https://doi.org/10.1021/acs.chemmater.7b02619>.

(27) Hörmann, N. G.; Guo, Z.; Ambrosio, F.; Andreussi, O.; Pasquarello, A.; Marzari, N. Absolute Band Alignment at Semiconductor-Water Interfaces Using Explicit and Implicit Descriptions for Liquid Water. *Npj Comput. Mater.* **2019**, *5* (1), 100. <https://doi.org/10.1038/s41524-019-0238-4>.

(28) Anh Pham, T.; Li, T.; Nguyen, H. V.; Shankar, S.; Gygi, F.; Galli, G. Band Offsets and Dielectric Properties of the Amorphous Si 3N4/Si(100) Interface: A First-Principles Study. *Appl. Phys. Lett.* **2013**, *102* (24), 241603. <https://doi.org/10.1063/1.4811481>.

(29) Pham, T. A.; Lee, D.; Schwegler, E.; Galli, G. Interfacial Effects on the Band Edges of Functionalized Si Surfaces in Liquid Water. *J. Am. Chem. Soc.* **2014**, *136* (49), 17071–17077. <https://doi.org/10.1021/ja5079865>.

(30) Gaiduk, A. P.; Govoni, M.; Seidel, R.; Skone, J. H.; Winter, B.; Galli, G. Photoelectron Spectra of Aqueous Solutions from First Principles. *J. Am. Chem. Soc.* **2016**, *138* (22), 6912–6915. <https://doi.org/10.1021/jacs.6b00225>.

(31) Wiktor, J.; Reshetnyak, I.; Ambrosio, F.; Pasquarello, A. Comprehensive Modeling of the Band Gap and Absorption Spectrum of BiVO₄. *Phys. Rev. Mater.* **2017**, *1* (2), 022401. <https://doi.org/10.1103/PhysRevMaterials.1.022401>.

(32) Cooper, J. K.; Gul, S.; Toma, F. M.; Chen, L.; Glans, P. A.; Guo, J.; Ager, J. W.; Yano, J.; Sharp, I. D. Electronic Structure of Monoclinic BiVO₄. *Chem. Mater.* **2014**, *26* (18), 5365–5373. <https://doi.org/10.1021/cm5025074>.

(33) Ping, Y.; Sundararaman, R.; Goddard, W. A. Solvation Effects on the Band Edge Positions of Photocatalysts from First Principles. *Phys. Chem. Chem. Phys.* **2015**, *17* (45), 30499–30509. <https://doi.org/10.1039/c5cp05740j>.

(34) Trasatti, S. The Absolute Electrode Potential: An Explanatory Note (Recommendations 1986). *Pure Appl. Chem.* **1986**, *58* (7), 955–966. <https://doi.org/10.1351/pac198658070955>.

(35) Gerosa, M.; Gygi, F.; Govoni, M.; Galli, G. The Role of Defects and Excess Surface Charges at Finite Temperature for Optimizing Oxide Photoabsorbers. *Nat. Mater.* **2018**, *17* (12), 1122–1127. <https://doi.org/10.1038/s41563-018-0192-4>.

(36) Govindaraju, G. V.; Wheeler, G. P.; Lee, D.; Choi, K. S. Methods for Electrochemical Synthesis and Photoelectrochemical Characterization for Photoelectrodes. *Chem. Mater.* **2017**, *29* (1), 355–370. <https://doi.org/10.1021/acs.chemmater.6b03469>.

(37) Hilbrands, A. M.; Zhang, S.; Zhou, C.; Melani, G.; Wi, D. H.; Lee, D.; Xi, Z.; Head, A. R.; Liu, M.; Galli, G.; Choi, K.-S. Impact of Varying the Photoanode/Catalyst Interfacial Composition on Solar Water Oxidation: The Case of BiVO_4 (010)/FeOOH Photoanodes. *J. Am. Chem. Soc.* **2023**, *145* (43), 23639–23650. <https://doi.org/10.1021/jacs.3c07722>.

